# Collisionless motion and evaporative cooling of atoms in magnetic traps

Surkov, E.L.; Walraven, J.T.M.; Shlyapnikov, G.V.

*Published in:*
Physical Review A

# Collisionless motion and evaporative cooling of atoms in magnetic traps

E. L. Surkov,[1] J. T. M. Walraven,[2] and G. V. Shlyapnikov[1,2]
[1]Russian Research Center Kurchatov Institute, Kurchatov Square, 123182 Moscow, Russia
[2]Van der Waals-Zeeman Institute, University of Amsterdam, Valckenierstraat 65-67, 1018 XE Amsterdam, The Netherlands
(Received 27 June 1995)

We analyze the collisionless motion of atoms in magnetic traps in relation to evaporative cooling. For the example of a long Ioffe quadrupole trap we investigate both the regular and stochastic regimes of motion. We emphasize a strong influence of the regime of collisionless motion on the process of evaporative cooling. For evaporation of atoms across an axial potential barrier the stochastic motion of atoms at energies above the barrier enables three-dimensional evaporation, i.e., particles acquiring in elastic collisions a total enery higher than the barrier height $E_0$ escape from the trap. The regular motion leads to axial evaporation: only atoms which due to collisions acquire an axial energy higher than $E_0$ leave the trap. The rate of axial evaporation is smaller by a factor $\sim \eta = E_0/T \gg 1$, where $T$ is the gas temperature. This has important consequences for evaporative cooling, which we discuss in relation to trapped atomic hydrogen.

PACS number(s): 32.80.Pj

## I. INTRODUCTION

Evaporative cooling is an important method to obtain ultralow temperatures in trapped atomic gases. The method was proposed to achieve Bose-Einstein condensation in atomic hydrogen [1]. Evaporative cooling was first demonstrated in hydrogen experiments [2–4]. Recently it has been applied to other trapped gases [5,6].

Evaporative cooling is based on the preferential removal of energetic atoms generated in interatomic collisions. The removal can be arranged with [7,5] or without [3,4,6] the use of electromagnetic radiation. To enable fast cooling, the experiments (see [3–6]) are carried out at the highest densities currently obtainable in atomic traps. Although at these densities interatomic collisions are frequent (on the time scale of the experiment), in all cases the mean free path of the atoms, $\lambda$, is much larger than the size $l$ of the samples,

$$\lambda \gg l \tag{1}$$

and accordingly the nonlinear dynamics of collisionless motion of the atoms can manifest itself. This was observed and investigated for processes that occur on a time scale short in comparison to the characteristic collisional time $\tau_c$ [3,8–11].

It is remarkable that under condition (1) the characteristic features of collisionless motion can also influence the process of evaporative cooling although the latter occurs on a time scale larger than $\tau_c$. If the removal of atoms is due to escape across a trap barrier the character of evaporation is determined by the collisionless motion at energies above the escape limit $E_0$. In the case of stochastic motion all particles with a total energy exceeding $E_0$ escape from the trap, and we have three-dimensional evaporation. In the case of regular motion evaporative cooling depends on the trapping geometry and can be such that only the particles for which the energy of motion in one (axial) direction exceeds $E_0$ can escape from the trap.

In this paper we analyze the influence of collisionless motion on the evaporation of atoms across an axial potential barrier. We use the example of a long Ioffe quadrupole trap [12,13] which, depending on the trap parameters, allows both stochastic motion leading to three-dimensional evaporation and regular motion providing axial evaporation. We present the range of parameters corresponding to the two regimes of motion and emphasize a very important difference between the two types of evaporation: The rate of axial evaporation is smaller by a factor $\sim \eta = E_0/T \gg 1$, where $T$ is the gas temperature. As a result of this, in atomic hydrogen, where the presence of intrinsic relaxational heating places a lower limit on achievable temperatures, the minimum achievable temperature for three-dimensional evaporation will be significantly lower than that in the case of axial evaporation.

## II. REGULAR MOTION—ADIABATIC APPROXIMATION

The long Ioffe quadrupole trap is characterized by radial $(x,y)$ motion proceeding much faster than the motion in the axial $(z)$ direction. In this case the particle motion can be described within the adiabatic approximation: the amplitude and frequency of radial oscillations adiabatically follow the axial coordinate $z$ of the moving particle, and the axial motion is governed by an effective potential $U(z)$, which is the sum of the trapping potential and the radial kinetic energy, both averaged over the radial oscillations. Nonadiabatic corrections can be considered as small perturbations of the axial motion in the potential $U(z)$.

In the Ioffe quadrupole trapping geometry the axial field $B_z$ is created by two dipole coils of radius $R$, separated by a distance $2L$. The coils have the $z$ axis as a common symmetry axis and carry parallel currents [12,13]. With a homogeneous field superimposed along the $z$ axis one has

$$B_z = B_0 + B_1 f(z), \tag{2}$$

where $f(z)$ is given in Ref. [14]. The radial field is created by four straight conductors (''Ioffe bars'') carrying currents in alternating directions. Neglecting the radial field of the dipole coils we have $B_x^2 + B_y^2 = \beta^2 \rho^2$, where $\rho = (x^2 + y^2)^{1/2}$.

 

We will assume that the spins of the moving atoms adiabatically follow the direction of the magnetic field. Then, the classical motion of an atom with magnetic moment $\mu$ antiparallel to the field is governed by the Hamiltonian

$$H=\mathbf{p}^2/2m+\mu(|\mathbf{B}|-B_0). \tag{3}$$

Two saddle points in the modulus of the magnetic field, $|\mathbf{B}|$, at $z=\pm L$, mark the axial evaporation barrier of the trap. With our approximation for the radial field the Hamiltonian (3) is axially symmetrical, which corresponds to the conservation of the projection $M$ of the orbital angular momentum on the $z$ axis. It is convenient to turn to dimensionless coordinate $\mathbf{r}/R\rightarrow\mathbf{r}$ and time $t\sqrt{\beta\mu/mR}\rightarrow t$, and to work with dimensionless field $\mathbf{B}/\beta R\rightarrow\mathbf{B}$ and Hamiltonian $H/\mu\beta R\rightarrow H$. From this point on we will work with these dimensionless variables and quantities unless otherwise stated.

In the case, where $B_1\ll B_0$ and the particle energy $E\ll B_0$, expanding the expression for the modulus of the magnetic field, $|\mathbf{B}|=\sqrt{B_z^2+x^2+y^2}$, in powers of $x$ and $y$ and retaining only quadratic terms, we arrive at the Hamiltonian $H=H_z+H_x+H_y$ with

$$H_z=\frac{p_z^2}{2}+B_1 f(z), \quad H_x=\frac{p_x^2}{2}+\frac{\omega^2(z)}{2}x^2 \tag{4}$$

and $H_y$ determined by the expression similar to that for $H_x$. The radial frequency

$$\omega(z)=1/\sqrt{B_z}\simeq\omega_0[1-\epsilon f(z)], \tag{5}$$

where $\omega_0=1/\sqrt{B_0}$ and $\epsilon=B_1/2B_0\ll 1$. We will demonstrate the adiabatic approximation for the Hamiltonian (4). The coupling between axial and radial motion is associated with the $z$ dependence of $\omega$. The fact that the axial motion is slow compared to the radial one can be expressed by the inequality

$$|\dot{\omega}|\ll\omega^2, \tag{6}$$

where $\dot{\omega}$ is the time derivative of the radial frequency. The equations of motion for $x$ and $y$ look similar to a Schrödinger equation with potential $\omega^2(z)$, and the condition (6) is nothing else than the WKB criterion. The corresponding quasiclassical solutions are

$$\begin{aligned} x&=\sqrt{2J_x/\omega(z)}\,\sin(\phi+\phi_{0,x}),\\ p_x&=\sqrt{2J_x\omega(z)}\,\cos(\phi+\phi_{0,x}),\\ y&=\sqrt{2J_y/\omega(z)}\,\sin(\phi+\phi_{0,y}),\\ p_y&=\sqrt{2J_y\omega(z)}\,\cos(\phi+\phi_{0,y}). \end{aligned} \tag{7}$$

Here $J_x\simeq$const and $J_y\simeq$const are approximate adiabatic invariants for $x$ and $y$ motion. The phase $\phi$ is determined by the expression

$$\phi=\int_0^t\omega(z(t'))dt'. \tag{8}$$

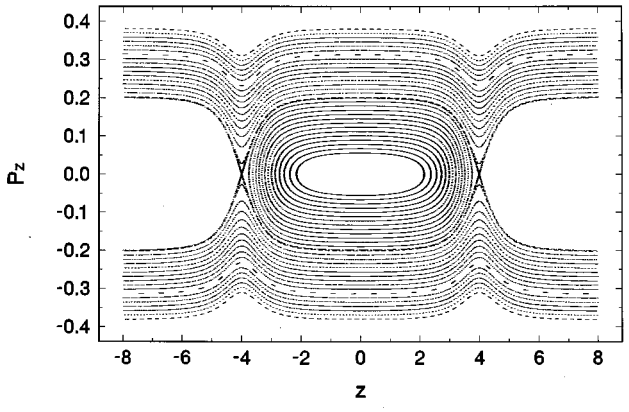


FIG. 1. Poincaré map with potential (11) for the case of regular motion: $B_0=0.1$, $B_1=0.025$, $E=0.075$, $M=0$.

From Eqs. (7) we have $H_x+H_y=J\omega(z)\simeq J\omega_0-J\omega_0\epsilon f(z)$, where $J=J_x+J_y$. Thus, with the radial motion determined by Eqs. (7), the axial motion will be governed by the adiabatic Hamiltonian

$$H_0=\frac{p_z^2}{2}+U(z), \tag{9}$$

where

$$U(z)\simeq E_s f(z) \tag{10}$$

is the axial potential renormalized due to the radial motion. The quantity $E_s=B_1-\epsilon J\omega_0$ is the energy at the escape limit, i.e., the energy on the separatrix (the curve in the phase space separating the region of finite axial motion from the region of infinite one).

The adiabatic approximation, with nonadiabatic corrections neglected, corresponds to regular coupling between axial and radial motion. The energy transfer from the radial degrees of freedom to the $z$ motion and back predominantly occurs in the spatial region near the coils where the $z$ dependence of the effective radial frequency $\omega$ is most important. Due to the condition $\epsilon\ll 1$ only a small fraction of the particle energy takes part in this energy exchange.

In Fig. 1 we present a Poincaré map for the Hamiltonian (3) rewritten in reduced cylindrical coordinates,

$$H=\frac{p_z^2}{2}+\frac{p_\rho^2}{2}+\frac{M^2}{2\rho^2}+\sqrt{B_z^2+\rho^2}-B_0 \tag{11}$$

($p_\rho$ is the momentum of radial oscillations) for $B_0=0.1$, $B_1=0.025$, $L=4$, $M=0$, and the total energy $E=3E_s=0.075$. For $E_z\geqslant E_s$, in order to make the motion finite, we put perfectly reflecting mirrors in the outer region of the trapping field at $z=\pm 2L$. The phase space of the Hamiltonian (11) is four dimensional. The surface of constant energy, $H=E=$const, determines a three-dimensional manifold in which the phase trajectory crosses the hyperplane $p_\rho=0$ in the direction $p_\rho>0$ and puts a mark as a point in the plane $(z,p_z)$. One can easily see that almost all phase trajectories are located on invariant thorae and only near the separatrix is

there a narrow stochastic layer. Similar results are obtained for the same trap parameters and $M \neq 0$.

### III. NONADIABATIC PERTURBATION AND STOCHASTIZATION OF MOTION

Stochastization of the motion can occur due to the presence of the saddle points at $z = \pm L$ in the trapping potential and the existence of nonadiabatic corrections to the solutions (7) for $x,y$ and $p_x,p_y$. These corrections result in a time-dependent perturbation that we should add to the Hamiltonian (9) of the axial motion. This perturbation is determined by $H_{\rm int} = H_x + H_y - J\omega(z)$ and has a frequency close to $2\omega_0$. It will be sufficient for us to consider the time variations of the energy $H_0$, caused by the nonadiabatic perturbation, without deriving the explicit expression for $H_{\rm int}$. For the time derivative of the Hamiltonian $H_0$ we obtain

$$\frac{dH_0}{dt} = \{H_0, H_{\rm int}\} = p_z \omega'(z)[J - \omega(z)(x^2 + y^2)]$$

$$= \omega'(z)\frac{dz}{dt}\left[\sum_{i=x,y} J_i \cos 2(\phi + \phi_{0,i})\right], \qquad (12)$$

where the symbol $\{\ \}$ denotes classical Poisson brackets, and for $x$ and $y$ we used Eqs. (7). From Eq. (12) one can see that the change of energy of the axial motion has a pulsed character and occurs during a finite time $\Delta t$, when the particle is moving in the region where the axial potential has its maximum slope and $\dot{\omega}$ is largest.

We will describe the stochastization of motion in the vicinity of the separatrix along the lines of a well-known mechanism discussed in the literature (see, e.g., [15]). Near the top of the axial potential barrier $U(z)$, i.e., in the vicinity of the saddle points at $z = \pm L$, the particle velocity in the $z$ direction is very small, and for both $E_z < E_s$ and $E_z > E_s$ (in the latter case we put perfectly reflecting mirrors at $z = \pm 2L$) just this region of $z$ determines the period of axial motion:

$$T_z(E_z) = \frac{4}{\Omega} \ln \frac{\sqrt{E_s} + \sqrt{E_z}}{\sqrt{|E_s - E_z|}} \ . \qquad (13)$$

Here $E_z$ is the energy of axial motion, and $\Omega^2 = E_s f''(L) = 3E_s$ is the curvature of the potential barrier $U(z)$ near its top. It is important that near the separatrix even a small nonadiabatic variation $\Delta H_0$ of the energy $E_z$ during the time $\Delta t$ can lead to such change of $T_z(E_z)$ that the corresponding change of the phase of the radial motion will be large:

$$\Delta\phi = \frac{\omega_0}{2}\frac{dT_z(E_z)}{dE_z}\Delta H_0 . \qquad (14)$$

The quantity $\Delta H_0$ depends on the phase of the radial motion, $\phi$. The stretching of a small phase interval is determined by the parameter of local instability, $K = |d\Delta\phi/d\phi|$. For $K \gtrsim 1$ there will be local instability in phases and, since the value and the sign of $\Delta H_0$ depend on the phase $\phi$, just this instability leads to stochastization of motion.

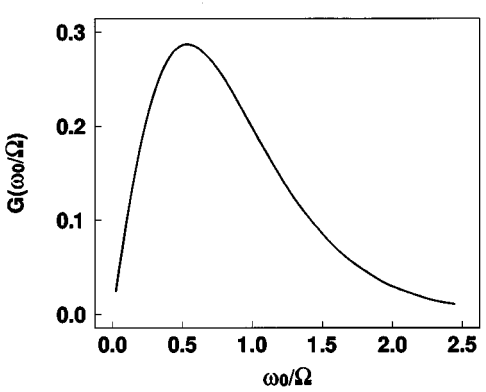


FIG. 2. The function $G$ vs $\omega_0/\Omega$.

In our case, by using Eq. (12) with $dz/dt$ on the separatrix, we obtain

$$\Delta H_0 = \int_{\Delta t} \frac{dH_0}{dt} dt = \epsilon G(\omega_0/\Omega) \sum_{i=x,y} J_i \Omega \cos 2(\phi_{0,i} + \phi). \qquad (15)$$

Then the parameter of local instability is given by

$$K = 2\epsilon \frac{G(\omega_0/\Omega)}{|E_s - E_z|}\left|\sum_{i=x,y} J_i \omega_0 \sin 2(\phi_{0,i} + \phi_n)\right|. \qquad (16)$$

The function $G(\omega_0/\Omega)$ was calculated numerically and is presented in Fig. 2. Its maximum value is achieved at $\omega_0/\Omega \approx 0.5$ and equals 0.28. For small values of the argument $G \simeq \omega_0/\Omega$, and for large values $G \simeq \exp(-2.35\omega_0/\Omega)$. From the condition $K \sim 1$ we obtain an estimate for the width of the stochastic layer near the separatrix:

$$\Delta E_z \simeq 2\epsilon E_\rho G\left(\frac{\omega_0}{\Omega}\right), \qquad (17)$$

where $E_\rho = J\omega_0$ is the characteristic energy of the radial motion. For axial energies in the range $|E_z - E_s| \lesssim \Delta E_z$ the parameter of local instability $K \gtrsim 1$ and the motion will be completely stochastic.

Due to the condition $\epsilon \ll 1$ corresponding to a small amplitude of the nonadiabatic perturbation, for $E_\rho \lesssim E_s$ the stochastic layer will be narrow for any ratio $\omega_0/\Omega$; i.e., the stochastic motion will occur only in a small part of the phase space near the separatrix. This conclusion is confirmed by Poincaré mapping for the potential (11) with perfectly reflecting mirrors at $z = \pm 2L$ (see also Fig. 1). The mapping shows that at energies comparable with $E_s$ (both $E_z \geqslant E_s$ and $E_z \leqslant E_s$) the motion is predominantly regular when the condition

$$\frac{B_1}{B_0} = 2\epsilon \ll 1 \qquad (18)$$

is satisfied.

The situation can be completely different if inequality (18) is not fulfilled. The results of our computer simulations show that at energies $\sim E_s$ we get a stochastic layer with

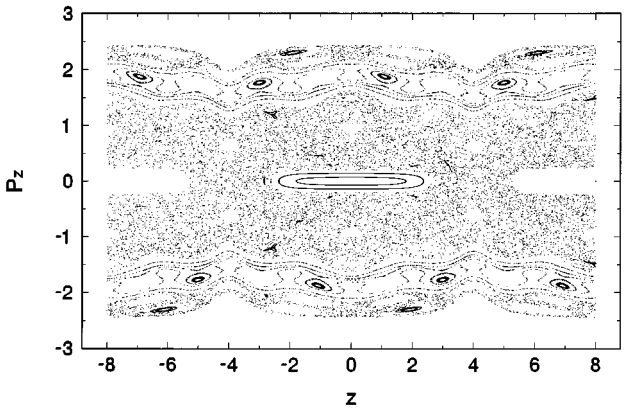


FIG. 3. Poincaré map with potential (11) for the case of stochastic sea: $B_0=0$, $B_1=1$, $E=3$, $M=0$.

width comparable to $E_s$, or even a stochastic sea (the stochastic motion occurs in the major part of the phase space), for the trap parameters

$$B_1 \gg B_0, \quad B_1 \sim 1. \tag{19}$$

This is the case for any projection of the orbital momentum except $M$ close to the maximum possible value at a given energy. In the range of $B_1$ and $B_0$, determined by Eq. (19), the adiabatic approximation breaks down. The amplitude of the nonadiabatic perturbation is sufficiently large and the characteristic frequency of the radial motion near the axial potential barrier is of the order of $\Omega$. The Poincaré map for the case of a stochastic sea is presented in Fig. 3. The mapping was performed with the potential (11) for $B_0=0$, $B_1=1$, $L=4$, $M=0$, and the total energy $E=3\approx 3E_s$.

## IV. AXIAL AND THREE-DIMENSIONAL EVAPORATION

Evaporative cooling is based on the preferential escape of energetic particles from the trap. For evaporation across a trap barrier the particles should, as a result of elastic collisions, acquire energies higher than the barrier height $E_0$. Both the number of particles and the gas energy decrease. But, since only energetic particles escape, the temperature goes down, causing the evaporation to be exponentially suppressed when $T \ll E_0$. The rate of evaporative cooling can be maintained by slowly ramping down the potential barrier (forced evaporative cooling). To increase the degeneracy parameter $n\Lambda_T^3$, where $\Lambda_T=(2\pi\hbar^2/mT)^{1/2}$ is the thermal de Broglie wavelength, the barrier should be ramped down at a rate slow compared to the rate of elastic collisions, but faster than any particle loss rate. Then, because the rate of evaporation will be small compared to the rate of elastic collisions, the gas will be in a quasiequilibrium.

The regime of collisionless motion at energies above $E_0$ is important for the character of evaporative cooling. If the motion is regular, then only the particles that acquire due to collisions an axial energy $E_z \geqslant E_0$ escape from the trap across the axial barrier. This type of evaporation we will call axial. In the case of completely stochastic motion at energies above $E_0$ we have three-dimensional evaporation; i.e., in order to escape from the trap it is enough for the particle to acquire a total energy $E \geqslant E_0$. This is just the case described in Fig. 3. Then, even if initially the axial energy was lower than $E_0$, the particle will escape because a strong collisionless mixing between axial and radial motion will necessarily make $E_z$ larger than $E_0$. Here we note that the characteristic mixing time, which can be larger than the period of axial motion, should be smaller than the characteristic collisional time $\tau_c$.

Returning to dimensional units, we will compare axial and three-dimensional evaporation assuming the same potential barrier $E_0$ for both cases. We consider a Boltzmann gas with a quasiequilibrium particle distribution corresponding to slowly time-dependent temperature. The rate of evaporation is the rate of elastic collisions in which one of the particles acquires an energy sufficiently high to escape from the trap. This rate can be found from kinetic theory. The collisionless motion only determines the type of evaporation. For axial evaporation both the radial energy $E_\rho$ of escaping particles and the range of axial energies above the barrier, $E_z-E_0$, will be $\sim T$. This type of evaporation is realized for the trap parameters from Eq. (18), as the width of the stochastic layer near the separatrix, given by Eq. (17), is much smaller than $T$. In the case of three-dimensional evaporation escaping particles have total energies in the range of the width $\sim T$ above $E_0$, and for realistic values $E_0/T \sim 5$ this type of evaporation takes place for the trap parameters from Eq. (19). For three-dimensional evaporation the quasiequilibrium distribution is truncated at total energy $E=E_0$. In the case of axial evaporation we have a thermal distribution of radial energies, and the distribution of axial energies is truncated at $E_z=E_0$.

Once the type of evaporation has been established, the rates of collisional processes can be calculated. For this calculation one only needs global information as contained in the density of states rather than the detailed shape of the potential. In the further analysis we will consider the trap configuration of the previous sections for $L \gg R$, which corresponds roughly to a square-root density of states for the axial motion. Assuming a linear density of states for the radial motion this is equivalent to calculating the collisional rates for a potential well, which is rectangular in the axial direction, with width $2L$ and height $E_0$, and harmonic in the radial direction, with frequency $\omega_0$. Then the particle and energy loss rates due to evaporation are determined by

$$\dot{N}_{\rm ev} = -\tfrac{1}{4} n_0^2 \sigma_{el} \overline{v}\, V_0 \exp(-\eta) f_N(\eta),$$

$$\dot{E}_{\rm ev} = -\tfrac{1}{4} n_0^2 \sigma_{el} \overline{v}\, V_0 E_0 \exp(-\eta) f_E(\eta), \tag{20}$$

with $V_0=2L(2\pi T/m\omega_0^2)$ being the characteristic gas volume in the trap, $\overline{v}=(8T/\pi m)^{1/2}$ the thermal velocity, $\sigma_{\rm el}$ ($\simeq 1.3\times 10^{-15}$ cm$^2$ for spin-polarized atomic hydrogen) the elastic cross section, $n_0$ the characteristic density [occupation numbers for particles in the trap are $(n_0\Lambda_T^3)\exp(-E/T)$] and the parameter $\eta=E_0/T$. The functions $f_N(\eta)$ and $f_E(\eta)$ for axial evaporation at $\eta \gtrsim 4$ are given by

$$f_{1N}(\eta) \simeq 1 - 1/\eta + 3/(2\eta^2),$$

$$f_{1E}(\eta) \simeq 1 + 3/(2\eta) - 2/\eta^2 \tag{21}$$

with an accuracy of 5%. In the case of three-dimensional

evaporation for the same values of $\eta$ and with the same accuracy we have

$$f_{3N}(\eta)\simeq 4\eta[1-7/(2\eta) + (4/3\sqrt{\pi})(\eta)^{3/2}(2/5+2/\eta)\exp(-\eta)]$$

and

$$f_{3E}(\eta)\simeq 4\eta[1-5/(2\eta)-9/(2\eta^2) + (24/35\sqrt{\pi})\eta^{3/2}(1+49/9\eta)\exp(-\eta)]$$

(cf. [16]).

The rate of axial evaporation is smaller by a factor of $\sim\eta$ than that in the case of three-dimensional evaporation:

$$\frac{f_{3N}}{f_{1N}}\simeq\frac{f_{3E}}{f_{1E}}\simeq 4\eta, \quad \eta\gg 1. \tag{22}$$

This difference originates from the ratio of the phase volumes responsible for axial and three-dimensional evaporation. We should also emphasize that in any trapping potential, allowing both types of evaporation, the phase volume of the axial evaporation is much smaller. Accordingly, the axial evaporation should proceed at a smaller rate than the three-dimensional one.

Let us now consider trapped atomic hydrogen and give an example how the difference between the rates of axial and three-dimensional evaporation should manifest itself in the characteristics of the evaporative cooling process. The lowest temperatures that can be reached in atomic hydrogen by evaporative cooling are limited by intrinsic heating associated with collisional dipolar relaxation in which two atoms with sufficiently small energies experience a spin flip and escape from the trap. The collisional relaxation mainly takes place in the high-density region near the axial center of the trap. The particle loss rate for both processes (evaporation and dipolar relaxation) has the same density dependence, $\dot{N}\sim n^2$, so there is a minimum temperature $T_{\min}$, independent of density, at which evaporative cooling and dipolar relaxation heating cancel each other. For the particle and energy flux $\dot{N}_{\rm dip}$ and $\dot{E}_{\rm dip}$ due to collisional dipolar relaxation we have

$$\dot{N}_{\rm dip}=-\tfrac{1}{2}n_0^2\alpha V_0 h_N(\eta),$$

$$\dot{E}_{\rm dip}=\dot{N}_{\rm dip}\,2Th_E(\eta), \tag{23}$$

with $\alpha$ being the dipolar rate constant ($\approx 10^{-15}$ cm$^3$/s for atomic hydrogen). In the case of axial evaporation the functions $h_N(\eta)$ and $h_E(\eta)$ are given by

$$h_{1N}=P^2(1/2,\eta),$$

$$h_{1E}=\left(1-\frac{1}{2P(1/2,\eta)}(\eta/\pi)^{1/2}\exp(-\eta)\right), \tag{24}$$

where $P(1/2,\eta)$ is an incomplete gamma function [for $\eta\gg 1$ we have $P^2(1/2,\eta)\simeq 1$]. For three-dimensional evaporation at $\eta\gtrsim 3$ we obtain with an accuracy of 1% (cf. [16]):

$$h_{3N}=1-[2(\eta/\pi)^{1/2}+5\eta/\pi]\exp(-\eta),$$

$$h_{3E}=1-[18\eta/\pi-7(\eta/\pi)^{1/2}]\exp(-\eta). \tag{25}$$

Internal energy of the trapped gas in our model is $E_{\rm int}=(5/2)NTP(7/2,\eta)/P(5/2,\eta)$ and the condition for the minimum achievable temperature, $\dot{T}=0$, leads to the equation

$$\dot{E}_{\rm int}=\dot{E}_{\rm ev}+\dot{E}_{\rm dip}=\tfrac{5}{2}T(\dot{N}_{\rm ev}+\dot{N}_{\rm dip}), \tag{26}$$

which can be solved numerically.

Now we compare $T_{1\min}$ calculated for the case of axial evaporation with $T_{3\min}$ characteristic for the case of three-dimensional evaporation. The result of comparison depends on the way of arranging evaporative cooling. Equation (26) gives a relation between $T_{\min}$ and the barrier height $E_0$ at the moment of time corresponding to the condition $\dot{T}=0$. In the case of evaporative cooling not forced by ramping down the

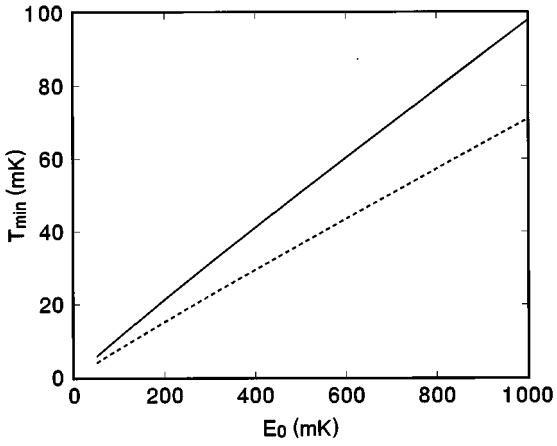


FIG. 4. Minimum achievable temperature $T_{\min}$ vs $E_0$ for evaporative cooling of atomic hydrogen at constant $E_0$. Solid curve corresponds to axial evaporation and dashed curve to three-dimensional evaporation.

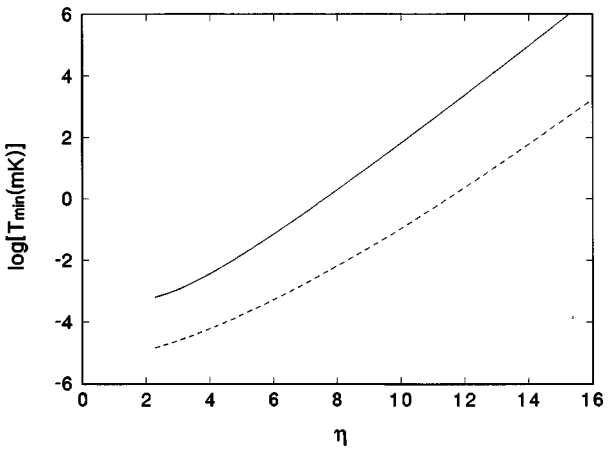


FIG. 5. Minimum achievable temperature $T_{\min}$ vs $\eta$ for forced evaporative cooling of atomic hydrogen ($\eta$=const). Solid curve corresponds to axial evaporation and dashed curve to three-dimensional evaporation.

barrier ($E_0 = \text{const}$) the preexponential factor in Eqs. (20) is much less important than the exponent, and $T_{1\min}$ will be only 10% or 20% higher than $T_{3\min}$ (see Fig. 4). For forced evaporative cooling keeping $\eta = \text{const}$ this preexponential factor is very important, and the minimum temperature will be a function of only the parameter $\eta$. In Fig. 5 we present $T_{1\min}(\eta)$ and $T_{3\min}(\eta)$. Comparing them with each other for the same value of $\eta$ one can see that in the range $6 \lesssim \eta \lesssim 10$, which is the most reasonable for evaporative cooling, axial evaporation leads to the minimum temperature more than an order of magnitude larger than that for three-dimensional evaporation. In a realistic procedure of evaporative cooling one is actually in between these two limiting cases, the minimum achievable temperature for axial evaporation being significantly higher than that for three-dimensional evaporation.

## ACKNOWLEDGMENTS

We acknowledge fruitful discussions with M.W. Reynolds. This work was enabled by the financial support of the Dutch Foundation for Fundamental Research of Matter FOM, Project No. NWO 07-30-002, the financial support by the project INTAS-93-2834, by Grant No. MMN000 from the International Science Foundation, and by Grant No. 94.02-04632 from the Russian Foundation for Basic Studies.

[1] H.F. Hess, Phys. Rev. B **34**, 3476 (1986).
[2] H.F. Hess, G. Kochanski, J.M. Doyle, N. Masuhara, D. Kleppner, and T.G. Greytak, Phys. Rev. Lett. **59**, 672 (1987).
[3] J.M. Doyle, J.C. Sandberg, I.A. Yu, C.L. Cesar, D. Kleppner, and T.J. Greytak, Phys. Rev. Lett. **67**, 603 (1991).
[4] O.J. Luiten, H.G.C. Werij, I.D. Setija, M.W. Reynolds, T.W. Hijmans, and J.T.M. Walraven, Phys. Rev. Lett. **70**, 544 (1993).
[5] W. Petrich, M.H. Anderson, J.R. Ensher, and E.A. Cornell, Phys. Rev. Lett. **74**, 3352 (1995).
[6] K.B. Davis, M-O. Mewes, M.A. Joffe, M.R. Andrews, and W. Ketterle, Phys. Rev. Lett. **74**, 5202 (1995); **75**, 2909(E) (1995).
[7] I.D. Setija, H.G.C. Werij, O.J. Luiten, M.W. Reynolds, T.W. Hijmans, and J.T.M. Walraven, Phys. Rev. Lett. **70**, 2257 (1993).
[8] C.R. Monroe, E.A. Cornell, S.A. Sackett, C.J. Myatt, and C.E. Wieman, Phys. Rev. Lett. **70**, 414 (1993).
[9] G.V. Shlyapnikov, J.T.M. Walraven, and E.L. Surkov, Hyperfine Interact. **76**, 31 (1993).
[10] *Antihydrogen*, edited by J. Eades (J.C. Baltzer AG, Basel, 1993).
[11] E.L. Surkov, J.T.M. Walraven, and G.V. Shlyapnikov, Phys. Rev. A **49**, 4778 (1994).
[12] Y.V. Gott, M.S. Ioffe, and G.V. Tel'kovski, Nucl. Fusion Suppl. **3**, 1045 (1962).
[13] D.E. Pritchard, Phys. Rev. Lett. **51**, 1336 (1983).
[14] The function $f(z)$ is given by
$$f(z) = \frac{g(z+L)+g(z-L)-2g(L)}{g(2L)+g(0)-2g(L)},$$
where $L$ is the distance from the symmetry center $z=0$ to each of the coils and $g(z) = [1+(z/R)^2]^{-3/2}$ is the axial magnetic field profile of a coil.
[15] G.M. Zaslavsky, R.Z. Sagdeev, D.A. Usikov, and A.A. Chernikov, *Weak Chaos and Quasi-Regular Patterns*, Cambridge Nonlinear Science Series 1 (Cambridge Univ. Press, Cambridge, 1991).
[16] O.J. Luiten, M.W. Reynolds, and J.T.M. Walraven, Phys. Rev. A **53**, 381 (1995).